Copy 5
RM L53A27
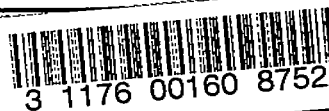
NACA RM L53A27

3 1176 00160 8752

# NACA

# RESEARCH MEMORANDUM

LOW-LIFT DRAG AND STABILITY DATA FROM ROCKET MODELS

OF A MODIFIED-DELTA-WING AIRPLANE WITH AND

WITHOUT EXTERNAL STORES AT MACH

NUMBERS FROM 0.8 TO 1.36

By Grady L. Mitcham and Willard S. Blanchard, Jr.

Langley Aeronautical Laboratory
Langley Field, Va.

CLASSIFICATION CHANGED

UNCLASSIFIED

To _____

By authority of _Nasa TPA 7_ Date _5-29-59_

_NB 7-7-59_

# NATIONAL ADVISORY COMMITTEE
# FOR AERONAUTICS
WASHINGTON
March 26, 1953

# NATIONAL ADVISORY COMMITTEE FOR AERONAUTICS

## RESEARCH MEMORANDUM

## LOW-LIFT DRAG AND STABILITY DATA FROM ROCKET MODELS

## OF A MODIFIED-DELTA-WING AIRPLANE WITH AND

## WITHOUT EXTERNAL STORES AT MACH

## NUMBERS FROM 0.8 TO 1.36

By Grady L. Mitcham and Willard S. Blanchard, Jr.

## SUMMARY

A flight investigation has been made to determine the drag and stability at low lift coefficients of models of a modified-delta-wing airplane at Mach numbers from 0.8 to 1.36 and a Reynolds number range from about $7 \times 10^6$ to $17 \times 10^6$. Included herein is a summary of the drag and stability data determined from these tests.

The drag break occurred at a Mach number of approximately 0.93 for the configurations tested. The external drag coefficient for the clean configuration was a constant value of about 0.010 at subsonic speeds and increased to about 0.038 at supersonic speeds. The addition of four rocket packets to the basic model resulted in very little increase in external drag coefficient. The addition of two external stores in combination with the four rocket packets, however, resulted in an increase in external drag coefficient of about 0.005 at subsonic speeds and 0.010 at supersonic speeds.

The transonic trim change, a pitching-up tendency, was mild. The slope of the lift curve varied smoothly throughout the Mach number range covered. The damping in pitch was low throughout the test Mach number range. The losses in duct total-pressure recovery between Mach numbers of 0.8 and 1.3 were small.

## INTRODUCTION

As a result of the current interest in the use of various triangular-wing plan forms for aircraft designed to fly at transonic and supersonic speeds, the National Advisory Committee for Aeronautics is conducting,

by use of rocket-powered models, drag and stability investigations of some of these configurations at large Reynolds numbers. The results from drag and stability investigations of a model of a 60° delta-wing airplane have been reported in references 1 and 2. In continuation of this program an investigation of some of the aerodynamic characteristics of an airplane configuration equipped with a 52.5° modified delta wing which incorporated a round-lip wing root inlet has been conducted. A summary of the results is presented herein.

The use of thin wings in high-speed fighter aircraft has increased interest in externally mounted fuel tanks and armament and their associated drag penalties. As a result, the primary purpose of the present investigation is to determine the drag of the basic airplane and the effect of the addition of external stores and rocket packets on the drag at low lift coefficients. One of the four models tested in this program was equipped with pulse rockets for disturbances in pitch in order to obtain some additional longitudinal stability derivatives. In addition to these data, some qualitative values of the directional-stability parameter and duct total-pressure recovery are presented.

## SYMBOLS

A                    duct exit area, sq ft

b                    wing span, ft

$\bar{c}$                    wing mean aerodynamic chord, ft

$C_{D_{internal}}$          internal drag coefficient

$C_{D_{base}}$            base drag coefficient (choking cup)

$C_{D_{total}}$            total drag coefficient

$C_{D_{external}}$          external drag coefficient,   $C_{D_{total}} - C_{D_{internal}} - C_{D_{base}}$

c.g.                 center-of-gravity location

$C_L$                  lift coefficient

$C_{L_\alpha}$                 lift-curve slope,  $\partial C_L / \partial \alpha$, per deg

$C_{L_{trim}}$              trim lift coefficient

$C_m$ pitching-moment coefficient about the center of gravity

$C_{m_{c/4}}$ pitching moment about the quarter chord of the mean aerodynamic chord

$(C_m)_{C_L=0,\delta=-0.3^\circ}$ pitching-moment coefficient at zero lift coefficient and $-0.3^\circ$ elevon deflection

$C_{m_\alpha}$ rate of change of pitching-moment coefficient with angle of attack, $\partial C_m/\partial \alpha$, per deg

$C_{m_q} + C_{m_{\dot\alpha}}$ pitch-damping factor, $\dfrac{\partial C_m}{\partial\left(\dfrac{\dot\theta\bar c}{2V}\right)} + \dfrac{\partial C_m}{\partial\left(\dfrac{\dot\alpha\bar c}{2V}\right)}$, per radian

$C_n$ yawing-moment coefficient

$C_{n_\beta}$ directional-stability parameter, $\partial C_n/\partial\beta$, per deg

$D$ drag, lb

$d$ diameter, ft

$H/H_0$ duct total-pressure recovery at station 24.3 with respect to free stream

$I_y$ moment of inertia about pitch axis, slug-ft$^2$

$I_z$ moment of inertia about yaw axis, slug-ft$^2$

$l$ length

$M$ free-stream Mach number

$m/m_0$ duct mass-flow ratio with respect to free stream and duct inlet area

$P$ period, sec

$p$ free-stream static pressure, lb/sq ft

$p_{exit}$ static pressure at the duct exit, lb/sq ft

$q$ free-stream dynamic pressure, lb/sq ft

$R$ Reynolds number based on wing mean aerodynamic chord

| | |
|---|---|
| S | wing area including body intercept, sq ft |
| V | free-stream velocity, ft/sec |
| $V_{exit}$ | velocity at duct exit, ft/sec |
| $T_{1/2}$ | time to damp to one-half amplitude, sec |
| x | horizontal distance from leading edge or nose |
| y | vertical distance measured from center line |
| $\delta$ | elevon deflection, deg |
| $\alpha$ | angle of attack at model center of gravity, deg |
| $\dot{\alpha}$ | rate of change of angle of attack with time, $\dfrac{1}{57.3}\dfrac{d\alpha}{dt}$, radians/sec |
| $\beta$ | angle of sideslip, deg |
| $\theta$ | angle of pitch, deg |
| $\dot{\theta}$ | rate of change of pitch angle, radians/sec |

All coefficients presented are based on a total wing area of 5.57 square feet with the exception of the store and pylon drag coefficients which are based on the maximum cross-sectional area of the store.

## MODELS AND APPARATUS

### Models

Four models of a turbojet-powered fighter airplane employing a 52.5° modified delta wing were used in this investigation. Two were of the clean configuration (one of these was disturbed in pitch), one had four rocket packets added, and the other was tested with four rocket packets and two Douglas Aircraft store shapes. A three-view drawing of the configurations tested is shown in figure 1(a) with the location and dimensions of the rocket packets and stores shown. Figure 1(b) presents a cutaway drawing of the clean configuration. Figures 2 to 4 are photographs of the models. Dimensional and mass characteristics of the models are given in table I. The models were constructed of wood with aluminum inserts and castings. Three pulse rockets to provide disturbances in pitch were installed in one of the clean models. These pulse rockets, two of which were located ahead and one behind the center of gravity, developed a total impulse of about 6 pound-seconds each with a burning time of approximately 0.08 second. A fixed elevon deflection of

0.3° trailing edge up was used and the trimmer inboard of the elevons was not deflected. The models were equipped with round-lip subsonic-design wing root inlets with two internal ducts merging together, thereby allowing the air to flow through and exhaust at the rear of the fuselage. In this paper the clean drag model is referred to as model 1 and the clean model with pulse rockets as model 2.

In order to determine the internal drag for each model with a minimum number of pressure measurements, a choking cup was designed and installed at the duct exit. This made it possible to obtain a Mach number of 1.0 at the exit during the supersonic part of the flight. A photograph of a typical choking-cup installation in one of the models is shown as figure 5. A more complete discussion of the technique used to determine internal drag is given in reference 3.

The four rocket packets were suspended below the wing by straight unswept pylons. Each pylon was 2.90 inches long and the thickness ratio was 5.74 percent. Details of these pylons can be found in table II. The rocket packets were cylindrical in cross section with an elliptical nose shape forward of 23.7 percent of the body length and a parabolic tail section rearward of 67.6 percent of the body length. The ordinates of these sections are given in table II. The maximum diameter of the rocket packets was 1.03 inches and the fineness ratio was 8.4.

Two straight unswept pylons were used to suspend the external stores below the wing. Each pylon was 3.15 inches long and had a thickness ratio of 10 percent. The two external stores were finned bodies of revolution having the standard Douglas Aircraft store shape. Each had a maximum body diameter of 2.1 inches at approximately 35 percent of the body length and a fineness ratio of 8.56. The body and pylon ordinates are given in table II and a revolved cross section of the pylon is given in figure 1(a). Two stores were also tested independently of the model. A photograph of one of the stores is shown in figure 6.

Each model was boosted to approximately M = 1.4 by a solid fuel, 6.25-inch-diameter Deacon rocket motor which produced an average thrust of 6500 pounds for about 3.0 seconds. None of the models contained an internal rocket sustainer motor. Launching was accomplished from the zero-length launcher seen in figure 7.

## Apparatus

During the flight of each model, a time history of the data was transmitted and recorded by means of a telemeter system. Eight channels of information were measured in each model. Model 1 and the model with rocket packets and external stores were instrumented to obtain normal,

longitudinal, and transverse acceleration, free-stream total pressure, inlet total pressure, inlet static pressure, exit static pressure, and choking-cup base pressure. In the model with only rocket packets, the transverse accelerometer was replaced by a free-stream static-pressure pickup. In model 2 the duct pressure pickups were replaced by an angle-of-attack vane and a reference pressure measured behind the angle-of-attack vane.

Free-stream temperature and static pressure were obtained from radiosondes released at time of firing. Ground apparatus consisted of a CW Doppler radar unit and a radar tracking unit which were used to determine the model velocity and position in space.

Free-flight drag data for the stores alone were obtained by accelerating the stores to low supersonic speeds by means of a 6-inch-bore compressed-helium gun and tracking them with a CW Doppler radar unit. Figure 8 shows a sketch of one of the model assemblies as it appeared prior to being accelerated through the gun barrel. The balsa cradles were used to aline the models in the gun barrel. Plywood push plates were used to transmit the pressure force to the assembly and to serve as a pressure seal while the assembly was in the barrel. Once free of the barrel, the cradles and push plates separated from the models.

A photograph of the compressed-helium gun is shown as figure 9. After the model assembly was mounted in the breech, helium gas under a pressure of 200 pounds per square inch was allowed to expand rapidly and accelerate the model assembly through the barrel and into free flight at supersonic speed.

## RESULTS AND DISCUSSION

The range of Reynolds number, based on the mean aerodynamic chord, covered by the tests varied from about $7 \times 10^6$ to $17 \times 10^6$ and is shown as a function of Mach number in figure 10.

The mass-flow ratios for the tests are given in figure 11. The mass flow for each model was regulated by means of the choking cup placed in the duct exit as discussed in a previous section. These mass-flow ratios for the models were varied by changing the choking-cup area.

The telemeter records indicated no buffet or flutter oscillations during the flight tests which were made at low lift coefficients.

## Lift

Lift-curve slope $C_{L_\alpha}$ as a function of Mach number is given in figure 12. These values of $C_{L_\alpha}$ were obtained by analysis of the pitch oscillations, which were the result of a disturbance associated with booster-model separation and the disturbances by the pulse rockets from the model equipped with the angle-of-attack vane (model 2). Tunnel results from the Ames 6- by 6-foot supersonic tunnel (ref. 4) and from the Southern California Cooperative Wind Tunnel (ref. 5) have been plotted in figure 12 for comparison. Agreement among these various sources is considered good with the best agreement occurring between the rocket-model test and the Ames 6- by 6-foot tunnel results.

The trim lift coefficients obtained with each model are given in figure 13. The change in $C_{L_{trim}}$ for the clean configurations (models 1 and 2) was small throughout the test speed range. The increment in $C_{L_{trim}}$ resulting from the addition of four rocket packets was small at transonic speeds and appeared to increase with increasing Mach number at supersonic speeds. The addition of the two Douglas Aircraft stores in conjunction with the four rocket packets, however, resulted in much larger increments in $C_{L_{trim}}$ throughout the Mach number range covered by the test. These increments changed sign near $M = 1.0$, being negative at subsonic speeds and positive at supersonic speeds.

## Drag

Values for internal drag coefficient are presented in figure 14. Since only the duct inlet was geometrically similar to the full-scale airplane internally, the values of internal drag coefficient are not applicable to the full-scale airplane but were used to determine the external drag coefficients. These values of internal drag coefficient, which were obtained by the method discussed in reference 3, are a small percentage of external drag.

The base drag coefficients $C_{D_{base}}$ of the choking cup for each of the models are given in figure 15. This drag also represents a very small portion of the external drag. Below $M = 0.93$, the gradual decrease in $C_{D_{base}}$ for the model with external stores is within the accuracy of the instruments.

The external drag coefficients for the models are shown in figure 16. These values of external drag were obtained by the relation

$$C_{D_{external}} = C_{D_{total}} - C_{D_{internal}} - C_{D_{base}}$$

The duct mass-flow ratios (fig. 11) for the models with external items and for clean model 1 were a constant value of about 0.5 throughout the test speed range. This value was changed to approximately 0.6 for the second clean configuration. As can be seen in figure 16, this change in mass-flow ratio had no measurable effect on external drag, since the differences in the drag values for the two models tested separately are within the accuracy of the data. It is believed, however, that if the mass-flow ratios had been varied by larger amounts there would have been a measurable effect of mass flow on external drag.

The drag break for all the configurations occurred at a Mach number of approximately 0.93 $\left(\text{determined by assuming that the drag break occurs where } \frac{dC_D}{dM} = 0.1\right)$ although the beginning of the drag rise for the model tested with two external stores in conjunction with four rocket packets was not so sharply defined as for the other tests. The small effect of external items on drag-break Mach number was also indicated by the wind-tunnel transonic-bump tests reported in reference 5.

The external drag coefficient for the clean configuration was nearly a constant value of 0.010 from $M = 0.8$ to $M = 0.93$, then increased abruptly to a value of 0.035 at $M = 1.0$, followed by a more gradual increase to a value of 0.038 at $M = 1.25$. One of these models (model 2) was tested primarily to obtain longitudinal-stability data; however, excellent agreement is shown between the external drag coefficients for the two models. Wind-tunnel results from tests of a 0.055-scale model in the Ames 6- by 6-foot supersonic wind tunnel (ref. 6) are shown plotted in figure 16 for comparison. The agreement between the rocket-model data and wind-tunnel data is considered to be good.

An estimate of the possible contributions of the various components to the over-all drag of the clean model indicated the body to be the main factor. The body drag was estimated by using the data of reference 7 and unpublished data. The wing and fin drags were estimated using the data of reference 8. At $M = 0.9$ the $\Delta C_D$ contributed by the body (including the wing fillet) was estimated to be about 40 percent of the total drag; whereas, at $M = 1.1$, this increment was increased to about 70 percent. The afterbody of the fuselage was sharply boattailed as shown in figure 1(b). Calculations indicate that it would be possible to reduce the over-all drag at low supersonic speeds by about 20 percent by a redesign of the afterbody behind the point of maximum thickness which would reduce the sharp boattail angle. The buckets in the drag curves at $M = 0.965$ are believed to be caused by pressure changes over the boattail which are probably the result of the formation of the shock wave on the afterbody. Tests of a parabolic body of revolution with a sharply convergent afterbody (ref. 9) indicated such changes of measured pressures over the boattail accompanied by buckets in the total drag coefficient. Results from

reference 10 indicate that a round-lip inlet of the type used on this
configuration tends toward a drag coefficient which increases with Mach
number well into the supersonic range.

The addition of four rocket packets resulted in only a small increase
in external drag coefficient (fig. 16) compared with that of the clean
configuration throughout the Mach number range covered by the test. The
addition of two external stores in conjunction with the four rocket
packets, however, resulted in increments of $C_D$ which varied from 0.005
at M = 0.8 to 0.008 at M = 1.0 and to 0.010 at M = 1.2, whereas,
the addition of rocket packets alone resulted in increments of $C_D$ of
less than 0.002 throughout the test speed range.

Drag coefficients based on the maximum cross-sectional area of the
store were obtained for the two Douglas Aircraft stores tested alone.
The results are presented as a function of Mach number in figure 17 and
wind-tunnel test values from reference 11 are given for comparison. The
drag coefficient for the store was approximately a constant value of 0.08
below the drag-break Mach number of 0.97, followed by an abrupt increase
in $C_D$ to 0.24 at M = 1.15. Also included in figure 17 are drag coef-
ficients for a store plus pylon and pylon alone. The pylon drag coef-
ficient, based on maximum cross-sectional area of the store, was esti-
mated from the results presented in reference 12. The increment in drag
caused by one store plus pylon was determined by subtracting the external
drag of the model with rocket packets from the external drag of the model
with rocket packets and external stores, dividing by 2, and relating to
store frontal area. The interference drag attributed to the store-plus-
pylon installation is almost twice the sum of the drag of the components.

Static Longitudinal Stability

The measured periods of the short-period longitudinal oscillations
in angle of attack and normal acceleration resulting from the disturbances
created by pulse rockets, booster-model separation, trim change, and
other random disturbances were used in determining the static-stability
parameters presented herein. The values of period for the four models
tested are shown in figure 18.

The values of period were used to calculate the static-longitudinal-
stability derivative $C_{m_\alpha}$ which is shown as a function of Mach number in
figure 19. The values for $C_{m_\alpha}$ were obtained by the method discussed in
reference 13. Since the method assumes linearities, the presented values
must be considered an average over the $C_L$ range covered by each test.
Tunnel tests from the Southern California Cooperative Wind Tunnel tran-
sonic bump (ref. 5) and the Ames 6- by 6-foot supersonic tunnel (ref. 4),

however, showed the existence of nonlinearities in the pitching moments
from $M = 0.8$ to $M = 1.02$ at the lift coefficients covered by the
rocket model tests. Above $M = 1.02$ the pitching moments were linear.
Two typical examples of the pitching moments (about $\bar{c}/4$) obtained from
the tunnel tests of the clean configuration are shown in figure 20; for
purposes of comparison, the rocket-model data have been corrected to
$\bar{c}/4$ and are shown in the same figure.

The aerodynamic-center location (fig. 21) for the flight tests was
obtained by use of the values for $C_{m_\alpha}$ and $C_{L_\alpha}$. There is considerable
difference in aerodynamic-center location for the various configurations
tested below $M = 1.1$. The differences in aerodynamic-center location may
be attributed to the nonlinearity of the pitching moments as discussed in
the previous paragraph or to cross-coupling between the pitch and lateral
oscillations which occurred simultaneously. In reference 14 evidence was
found to indicate that cross-coupling occurred between pitch and lateral
oscillations in the low angle-of-attack range. The effect of the external
items on the aerodynamic-center location could not be ascertained as a
result of the limitations previously discussed. Tunnel data from refer-
ences 5 and 6 indicated, however, that the addition of external items
had but small effect on the aerodynamic-center location at the low lift
coefficients. Below $M = 1.1$ the curves for aerodynamic-center location
are dashed because of the nonlinearity of the pitching moments and the
cross-coupling.

Pitching-moment coefficients at zero lift with $0.3^\circ$ trailing-edge-up
elevon deflection are shown in figure 22 for the four rocket models
tested. The two models of the clean configuration tested indicated neg-
ative values of pitching moments of about $-0.002$ at subsonic speeds and
positive values of about $0.003$ at supersonic speeds. The model with
rocket packets and the model with stores and rocket packets showed values
three and four times as large, respectively. Pitching-moment coefficients
at zero lift with $0.3^\circ$ trailing-edge-up elevon deflection determined from
the test results of the Ames 6- by 6-foot supersonic wind tunnel are
plotted in figure 22 for comparison. The agreement between the rocket-
model data and tunnel data is considered good.

Damping in Pitch

The damping-in-pitch parameters $T_{1/2}$ and $C_{m_q} + C_{m_{\dot\alpha}}$ which are
presented in figures 23 and 24, respectively, were obtained by analysis
of the rate of decay of the transient longitudinal oscillations resulting
from the disturbances created by the pulse rockets, booster-model separa-
tion, and the transonic trim change.

As previously stated, one of the models was equipped with pulse rockets in order to obtain additional longitudinal-stability data. The damping and stability data obtained from the three models used in the drag investigation were obtained by the analysis of a fairly large amplitude longitudinal oscillation which occurred at booster-model separation and smaller longitudinal oscillations resulting from the transonic trim change and other random means. The small amplitude oscillations (less than 0.5°) were very poorly damped; whereas, the damping derivatives obtained from an analysis of the larger amplitude oscillations showed better damping. One factor which may contribute to the reduced pitch damping could be the result of cross-coupling with a lateral oscillation that occurred simultaneously with and at the same frequency as the pitch oscillation below $M = 0.95$. The differences in $C_{m_q} + C_{m_{\dot{\alpha}}}$ resulting from the analysis of the small and larger amplitude pitch oscillations can be seen in figure 24. Unpublished results from tests of an aspect-ratio-3 53° sweptback delta wing tested in the Ames 6- by 6-foot supersonic wind tunnel are plotted in figure 24 for comparison. These results also indicate low damping at supersonic speeds and a larger reduction as transonic speeds are approached.

The damping of this airplane configuration is much less than the damping of a 60° delta-wing airplane model reported in references 1 and 2. The leading-edge sweep of 52.5° as compared with 60° in references 1 and 2 and the modification of the delta wing, which included sweeping back the trailing edge, are the significant differences between the two models which may contribute to the reduced damping.


### Directional Stability

As previously mentioned, three of the models were instrumented to record lateral force. Lateral oscillations induced by disturbances at booster separation, by trim change near $M = 1.0$, and, possibly, by rough air appeared on the recorded flight time histories of these models. The period of these oscillations is given in figure 25. These oscillations have been analyzed by the single-degree-of-freedom method of reference 15 using the following equation:

$$C_{n_\beta} = \frac{4\pi^2 I_z}{P^2 q S b}$$

This equation given for $C_{n_\beta}$ is qualified in reference 15 as applying primarily to conventional designs. Method 3 of the same reference,

however, presents a solution which includes the comparatively small-order stability derivatives which are neglected in the above equation. Values of $C_{n_\beta}$ obtained by this alternate method showed very good agreement with those obtained by the given equation. This indicated that, for this configuration, the errors in $C_{n_\beta}$ due to neglecting the small-order stability derivatives were so small that the equation given previously was sufficiently accurate. Values of $C_{n_\beta}$, the rate of change of yawing moment with respect to sideslip, are shown in figure 26. Wind-tunnel results from tests of a 0.055-scale model of this airplane in the Ames 6- by 6-foot supersonic wind tunnel (ref. 6), corrected to a center-of-gravity position of 16.5 percent of the mean aerodynamic chord, have been plotted in this figure for comparison. Figure 26 shows a reduction in $C_{n_\beta}$ at Mach numbers between 0.95 and 1.15. The reason for this apparent decrease is not known. Data from the model with the center-of-gravity location of $0.171\bar{c}$ indicated that the $C_{n_\beta}$ values in the Mach number range between 0.85 and 0.98 were, possibly, erroneously high because of cross-coupling with an oscillation in pitch that is known to have occurred simultaneously with and at the same frequency as the lateral oscillation. A subsequent test, however, indicated that this apparent cross-coupling was not eliminated when the mass characteristics and center of gravity of the model were adjusted (center-of-gravity location of $0.099\bar{c}$) so that the pitch and yaw natural frequencies were not equal, since the general nature of the variation of $C_{n_\beta}$ with Mach number did not change. The maximum angle of sideslip $\beta$ of the models was approximately $\pm 1^\circ$.

## Total-Pressure Recovery

Three of the models tested in this investigation had a total-pressure tube and a static-pressure orifice located in the duct at a station 9.70 inches behind the inlet. The purpose of these pressure tubes was to determine whether twin-duct flow instability existed for the two ducts discharging into a common duct. No twin-duct flow instability was indicated.

The location of each total-pressure tube with respect to the duct wall is shown in figure 27 and was different for each model in order to get some indication of the profile of the total pressure across the duct at the station 9.70 inches behind the inlet. Since a thorough duct total-pressure survey was not made, the values of total-pressure recovery presented in figure 27 are qualitative but indicate only small losses in total-pressure recovery between Mach numbers of 0.80 and 1.3.

CONCLUSIONS

The results obtained from flight tests at low lift coefficients of rocket models of an airplane configuration with and without external stores from a Mach number of 0.8 to 1.36 indicate the following conclusions:

1. The drag-break Mach number was approximately 0.93 for all configurations. The external drag coefficient for the clean configuration was nearly a constant value of 0.010 from M = 0.8 to M = 0.93, then increased abruptly to a value of 0.035 at M = 1.0, followed by a more gradual increase to a value of 0.038 at M = 1.25. The increment in drag coefficient resulting from the addition of four rocket packets was less than 0.002 throughout the test speed range; whereas, the addition of two external stores to the four rocket packets resulted in $C_D$ increments of 0.005, 0.008, and 0.010 at Mach numbers of 0.8, 1.0, and 1.2, respectively.

2. The drag coefficient for the Douglas Aircraft stores (based on maximum cross-sectional area), which were tested independently of the model, was approximately a constant value of 0.08 below the drag-break Mach number which occurred at 0.97 then increased abruptly to 0.24 at M = 1.15. The interference drag attributed to the store-plus-pylon installation on the model was almost twice the sum of the drag of the isolated store and isolated pylon.

3. The transonic trim change, a mild pitching-up tendency, occurred at about M = 0.93.

4. There were no large variations in lift-curve slope throughout the Mach number range of the tests.

5. Nonlinearities in the pitching moments resulted in considerable difference in aerodynamic-center location for the various configurations at any constant Mach number below M = 1.1.

6. The damping in pitch was low throughout the Mach number range.

7. Losses in duct total-pressure recovery between M = 0.8 and M = 1.3 were small.

8. No buffet or flutter oscillations were indicated during the flight tests which were at low lift coefficients.


Langley Aeronautical Laboratory,
    National Advisory Committee for Aeronautics,
        Langley Field, Va.

REFERENCES

1. Mitcham, Grady L., Stevens, Joseph E., and Norris, Harry P.:
   Aerodynamic Characteristics and Flying Qualities of a Tailless
   Triangular-Wing Airplane Configuration As Obtained From Flights of
   Rocket-Propelled Models at Transonic and Low Supersonic Speeds.
   NACA RM L9L07, 1950.

2. Mitcham, Grady L., Crabill, Norman L., and Stevens, Joseph E.: Flight
   Determination of the Drag and Longitudinal Stability and Control
   Characteristics of a Rocket-Powered Model of a 60° Delta-Wing Air-
   plane From Mach Numbers of 0.75 to 1.70.  NACA RM L51I04, 1951.

3. Faget, Maxime A., Watson, Raymond S., and Bartlett, Walter A., Jr.:
   Free-Jet Tests of a 6.5-Inch-Diameter Ram-Jet Engine at Mach Numbers
   of 1.81 and 2.00.  NACA RM L50L06, 1951.

4. Smith, Willard G.:  Wind-Tunnel Investigation at Subsonic and Super-
   sonic Speeds of a Model of a Tailless Fighter Airplane Employing a
   Low-Aspect-Ratio Swept-Back Wing - Stability and Control.  NACA
   RM A52J30, 1953.

5. Anon.:  Report on Wind-Tunnel Tests at Transonic Speeds of a $\frac{1}{40.2}$
   Scale Left-Hand Reflection-Plane Model of the Douglas 571 Airplane.
   CWT Rep. 115, Southern Calif. Cooperative Wind Tunnel, Sept. 27, 1949.

6. Smith, Willard G.:  Wind-Tunnel Investigation at Subsonic and Super-
   sonic Speeds of a Model of a Tailless Fighter Airplane Employing a
   Low-Aspect-Ratio Swept-Back Wing - Effects of External Fuel Tanks
   and Rocket Packets on the Drag Characteristics.  NACA RM A52J31,
   1953.

7. Hart, Roger G., and Katz, Ellis R.:  Flight Investigations at High-
   Subsonic, Transonic, and Supersonic Speeds To Determine Zero-Lift
   Drag of Fin-Stabilized Bodies of Revolution Having Fineness Ratios
   of 12.5, 8.91, and 6.04 and Varying Positions of Maximum Diameter.
   NACA RM L9I30, 1949.

8. Morrow, John D., and Nelson, Robert L.:  Large-Scale Flight Measure-
   ments of Zero-Lift Drag of 10 Wing-Body Configurations at Mach Num-
   bers From 0.8 to 1.6.  NACA RM L52D18a, 1953.

9. Stoney, William E., Jr.:  Pressure Distributions at Mach Numbers From
   0.6 to 1.9 Measured in Free Flight on a Parabolic Body of Revolution
   With Sharply Convergent Afterbody.  NACA RM L51L03, 1952.

10. Sears, Richard I., and Merlet, C. F.: Flight Determination of the Drag and Pressure Recovery of an NACA 1-40-250 Nose Inlet at Mach Numbers From 0.9 to 1.8. NACA RM L50L18, 1951.

11. Muse, T. C., and Bratt, R. W.: Summary of High Speed Wind-Tunnel Tests of a Douglas Aircraft Store Shape and a 2000-Pound G.P.-AN-M66 Bomb. Rep. No. E.S. 21150, Douglas Aircraft Co., Inc., June 25, 1948.

12. Danforth, Edward C. B.: A Correlation of Experimental Zero-Lift Drag of Rectangular Wings With Symmetrical NACA 65-Series Airfoil Sections by Means of the Transonic Similarity Law for Wings of Finite Aspect Ratio. NACA RM L51G20, 1951.

13. Gillis, Clarence L., Peck, Robert F., and Vitale, A. James: Preliminary Results From a Free-Flight Investigation at Transonic and Supersonic Speeds of the Longitudinal Stability and Control Characteristics of an Airplane Configuration With a Thin Straight Wing of Aspect Ratio 3. NACA RM L9K25a, 1950.

14. Chapman, Rowe, Jr., and Morrow, John D.: Longitudinal Stability and Drag Characteristics at Mach Numbers From 0.70 to 1.37 of Rocket-Propelled Models Having a Modified Triangular Wing. NACA RM L52A31, 1952.

15. Bishop, Robert C., and Lomax, Harvard: A Simplified Method for Determining From Flight Data the Rate of Change of Yawing-Moment Coefficient With Sideslip. NACA TN 1076, 1946.

16. Toll, Thomas A., and Queijo, M. J.: Approximate Relations and Charts for Low-Speed Stability Derivatives of Swept Wings. NACA TN 1581, 1948.

17. Ribner, Herbert S., and Malvestuto, Frank S., Jr.: Stability Derivatives of Triangular Wings at Supersonic Speeds. NACA Rep. 908, 1948. (Supersedes NACA TN 1572.)

TABLE I

PHYSICAL CHARACTERISTICS OF THE MODELS

Wing:
   Area (included), sq ft . . . . . . . . . . . . . . . . . . . . . 5.57
   Span, ft . . . . . . . . . . . . . . . . . . . . . . . . . . . 3.35
   Aspect ratio . . . . . . . . . . . . . . . . . . . . . . . . . 2.01
   Mean aerodynamic chord, ft . . . . . . . . . . . . . . . . . . 1.82
   Sweepback of leading edge, deg . . . . . . . . . . . . . . . . 52.5
   Dihedral (relative to mean thickness line), deg . . . . . . . . . 0
   Taper ratio (tip chord/root chord) . . . . . . . . . . . . . . 0.33
   Airfoil section at center line   . . . .   NACA 0007-63/30 - 9.5° mod.
   Airfoil section at tip . . . . . . . .   NACA 0004.5-63/30 - 6.6° mod.

Vertical tail:
   Area (extended to center line), sq ft . . . . . . . . . . . . 0.48
   Aspect ratio . . . . . . . . . . . . . . . . . . . . . . . . . 2.08
   Height (above fuselage center line), ft . . . . . . . . . . . . 1.00
   Sweepback of leading edge, deg . . . . . . . . . . . . . . . . 66.6
   Taper ratio (tip chord/root chord) . . . . . . . . . . . . . . 0.26
   Airfoil section at root  . . . . . . . . . . .   NACA 0008-63/30 - 9°
   Airfoil section at tip . . . . . . . . . . .   NACA 0006-63/30 - 6° 45'

Elevon:
   Area (one), sq ft  . . . . . . . . . . . . . . . . . . . . . 0.23
   Span (one), ft . . . . . . . . . . . . . . . . . . . . . . . . 1.12
   Chord, ft  . . . . . . . . . . . . . . . . . . . . . . . . . 0.22

Ducts:
   Inlet area, sq in.   . . . . . . . . . . . . . . . . . . . 6.10
   Exit area, sq in.
     (except clean model 2) . . . . . . . . . . . . . . . . . . . 3.46
     (clean model 2)  . . . . . . . . . . . . . . . . . . . . . 4.45
   Choking-cup area, sq in.
     (except clean model 2) . . . . . . . . . . . . . . . . . . . 3.05
     (clean model 2)  . . . . . . . . . . . . . . . . . . . . . 2.06

TABLE I - Concluded

PHYSICAL CHARACTERISTICS OF THE MODELS

Weight and balance:

|  | Clean model 1 | Clean model 2 | Clean + rocket packets | Clean + packets + stores |
|---|---|---|---|---|
| Weight, lb . . . . . . . . . . | 109.94 | 122.25 | 110.31 | 112.94 |
| Wing loading, lb/sq ft . . . . | 19.75 | 21.93 | 19.81 | 20.25 |
| Center-of-gravity position, percent $\bar{c}$ . . . . . . . . . | 16.5 | 9.91 | 16.9 | 17.15 |
| Moment of inertia in pitch, slug-ft$^2$ . . . . . . . . . . | 3.90 | 4.69 | 3.90 | 3.94 |
| Moment of inertia in yaw, slug-ft$^2$ . . . . . . . . . . | 4.56 | 5.37 | ------ | 4.56 |

## TABLE II

### ORDINATES FOR EXTERNAL STORES, ROCKET PACKETS, AND PYLONS

| External store | | Store pylon | | Rocket packet | | Packet pylon | |
|---|---|---|---|---|---|---|---|
| $x/l$ | $y/l$ | $x/l$ | $y/l$ | $x/l$ | $y/l$ | $x/l$ | $y/l$ |
| 0 | 0 | 0 | 0 | 0 | 0 | 0 | 0 |
| .019 | .009 | .01 | .010 | .05 | .032 | .05 | .016 |
| .047 | .020 | .02 | .014 | .10 | .048 | .10 | .022 |
| .075 | .029 | .05 | .022 | .15 | .056 | .15 | .027 |
| .103 | .035 | .10 | .031 | .24 | .060 | .22 | .028 |
| .130 | .040 | .20 | .041 | .30 | .060 | .30 | .028 |
| .158 | .044 | .30 | .047 | .40 | .060 | .40 | .028 |
| .186 | .047 | .40 | .050 | .50 | .060 | .50 | .028 |
| .204 | .050 | .45 | .050 | .60 | .060 | .60 | .028 |
| .242 | .053 | .55 | .048 | .68 | .060 | .65 | .028 |
| .270 | .055 | .65 | .043 | .70 | .059 | .71 | .027 |
| .297 | .057 | .75 | .034 | .72 | .058 | .75 | .025 |
| .325 | .057 | .85 | .021 | .75 | .057 | .80 | .022 |
| .353 | .058 | .95 | .007 | .77 | .055 | .85 | .017 |
| .425 | .058 | 1.00 | 0 | .79 | .053 | .90 | .012 |
| .497 | .058 | | | .82 | .051 | .95 | .007 |
| .525 | .058 | T.E. radius = | | .84 | .048 | .98 | .004 |
| .553 | .057 | 0.0055$l$ | | .86 | .044 | 1.00 | 0 |
| .580 | .056 | | | .88 | .040 | | |
| .637 | .053 | | | .91 | .035 | | |
| .691 | .049 | | | .93 | .029 | | |
| .748 | .043 | | | .95 | .023 | | |
| .803 | .037 | | | .98 | .016 | | |
| .858 | .030 | | | .99 | .011 | | |
| .914 | .022 | | | 1.00 | 0 | | |
| .958 | .016 | | | | | | |
| .980 | .012 | | | | | | |
| 1.000 | 0 | | | | | | |
| T.E. radius = | | | | | | | |
| 0.0055$l$ | | | | | | | |
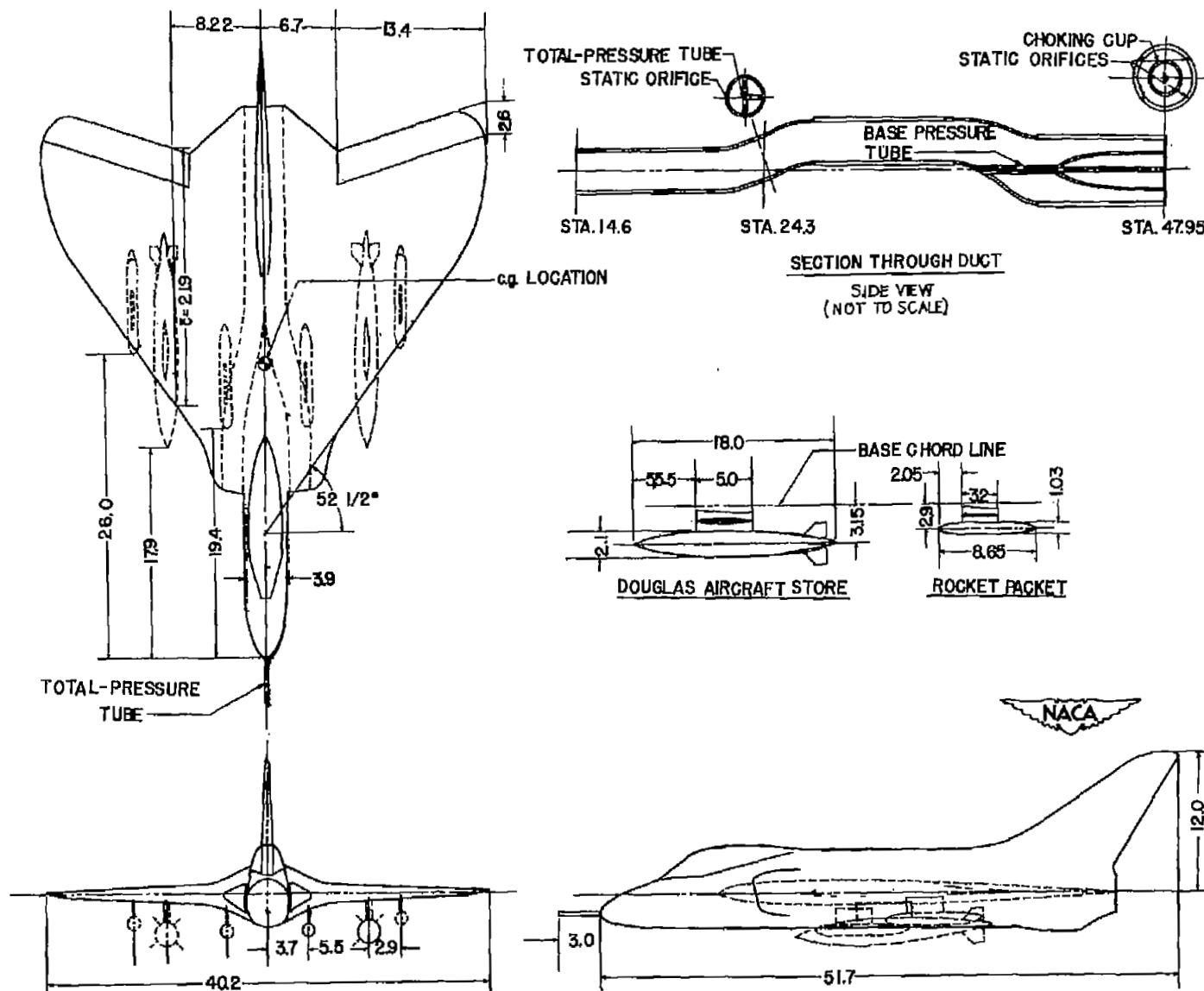
(a) Three-view drawing of the model and the external items. All dimensions are in inches.

Figure 1.- Views of model.

(b) Cutaway drawing of the model.

Figure 1.- Concluded.
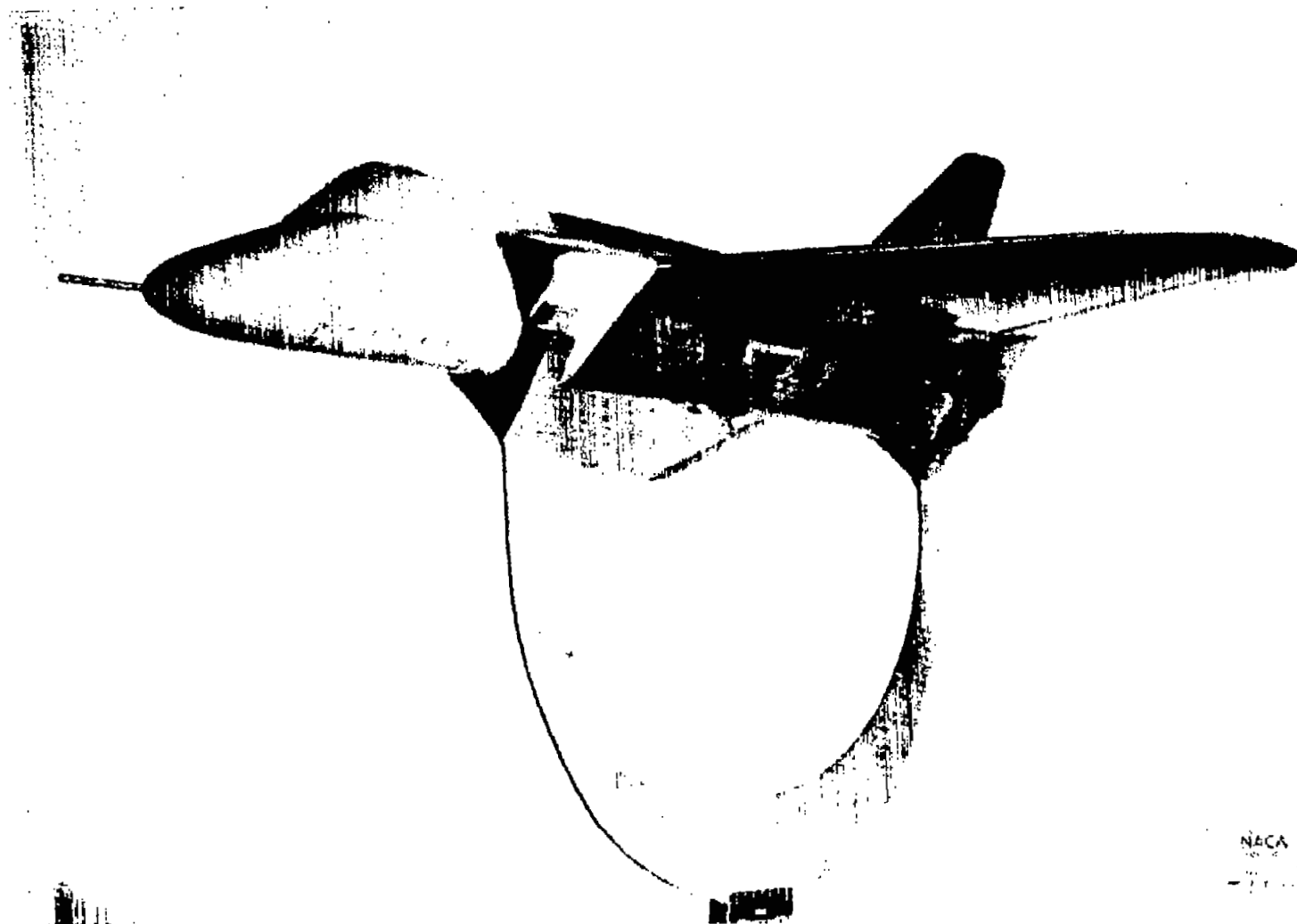
Figure 2.- Photograph of one of the clean models.
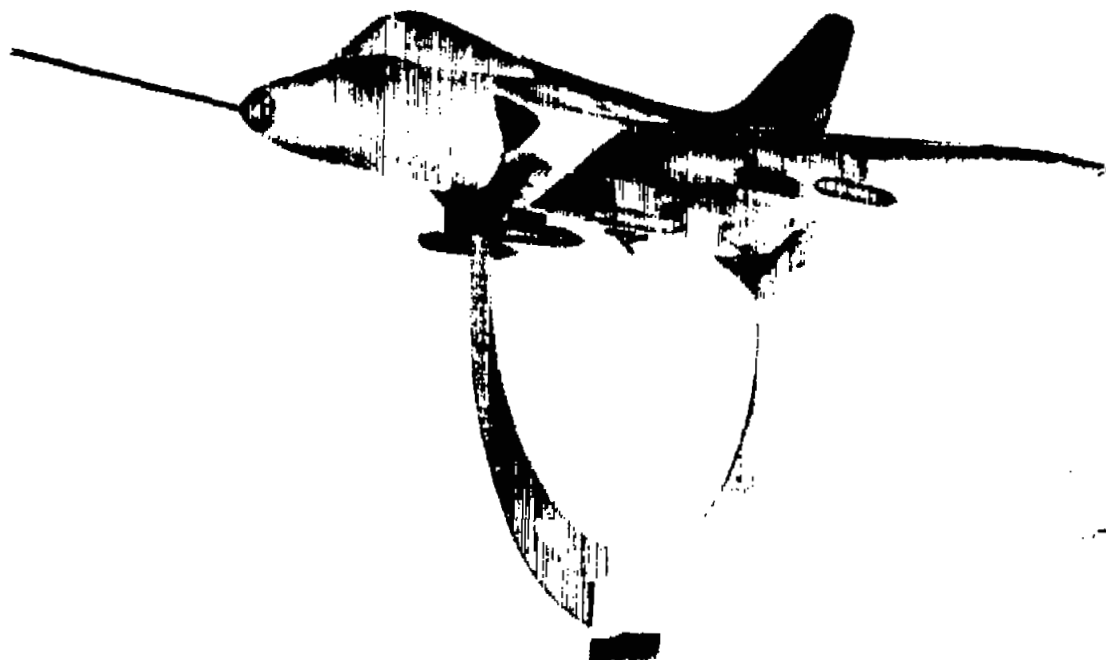
NACA

Figure 3.- Model with four rocket packets.
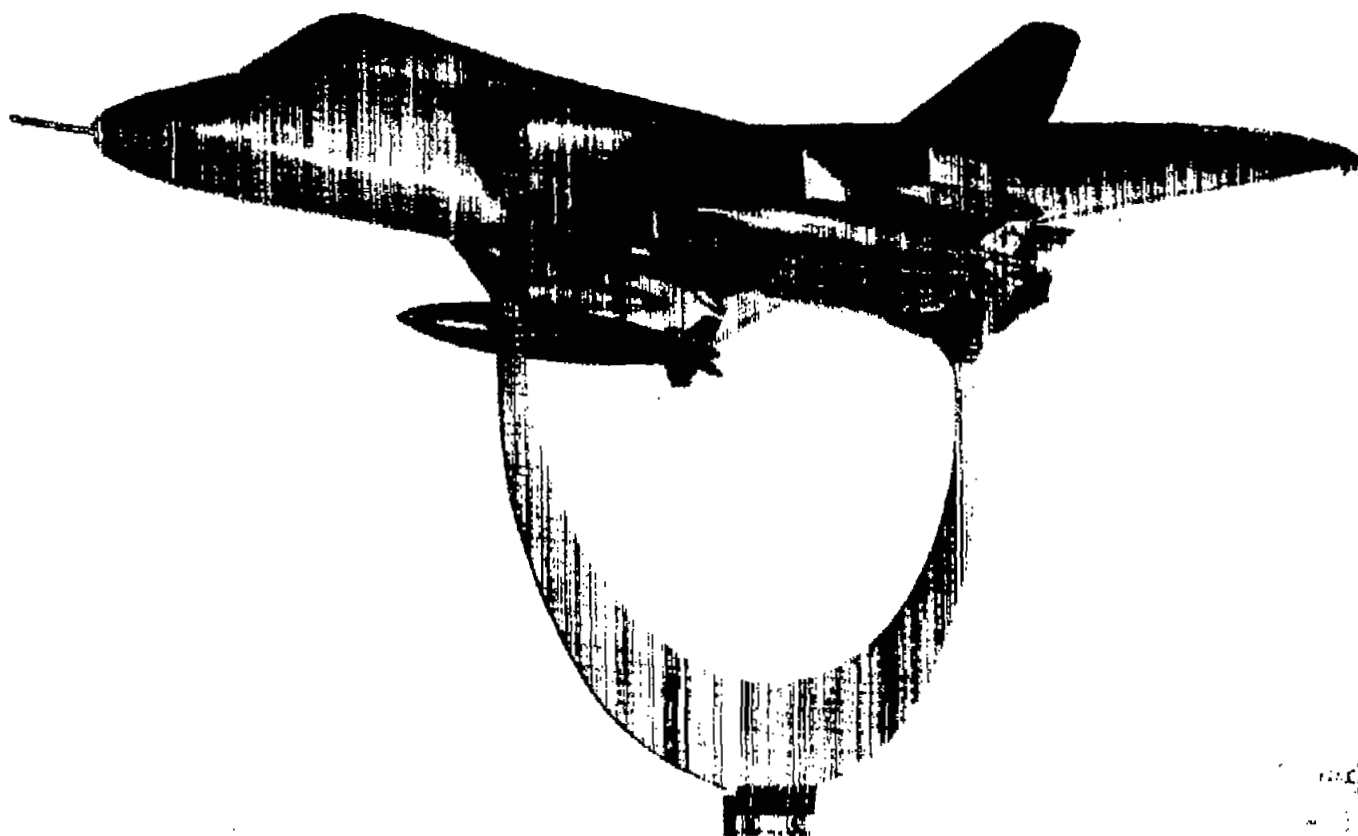
Figure 4.- Model with four rocket packets and two external stores.

Figure 5.- Typical choking-cup installation in one of the models.
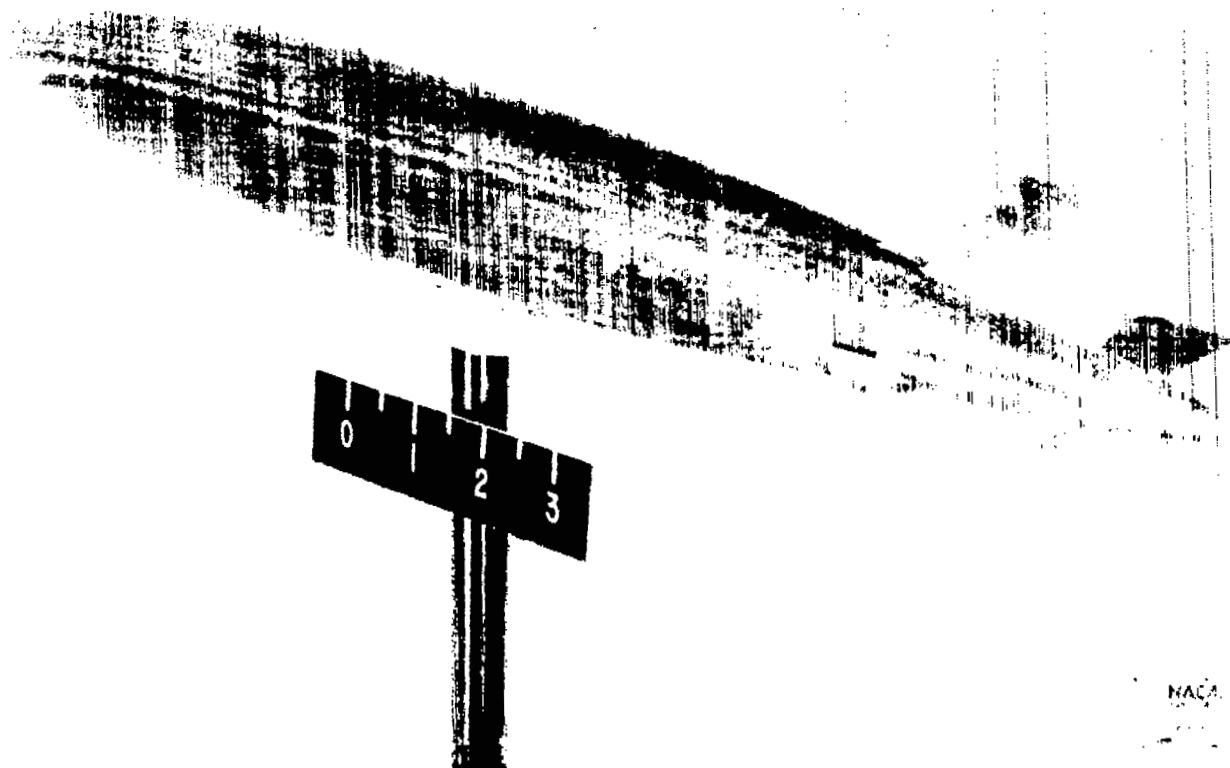
Figure 6.- One of the stores tested in the compressed-helium gun.
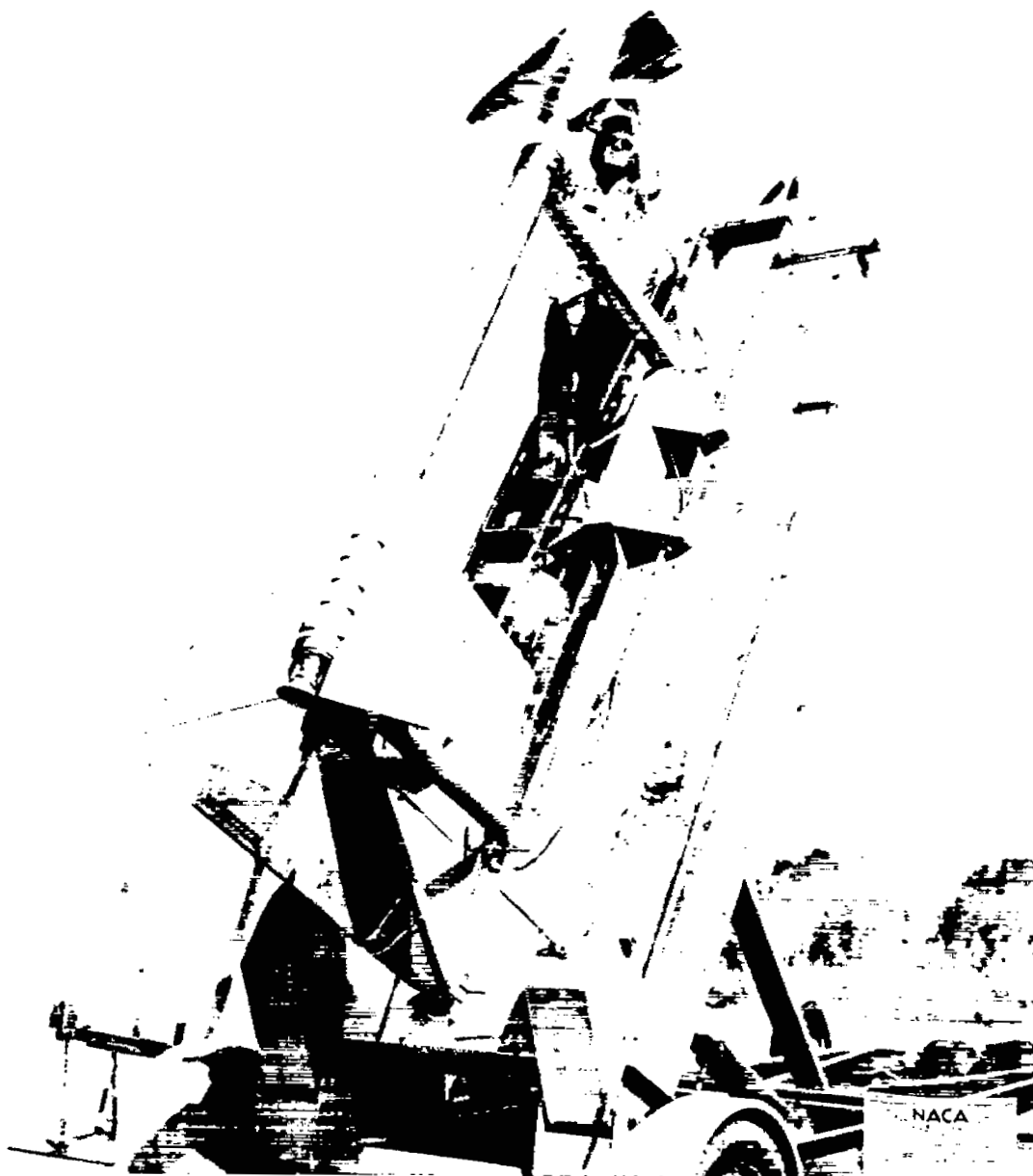
Figure 7.- One of the booster-model combinations in launching position.

Balsa cradle (4 sections)

Douglas Aircraft Store

Plywood push plate
with duralumin inserts

3.0

6.0

2.0   8.0   2.0   .75
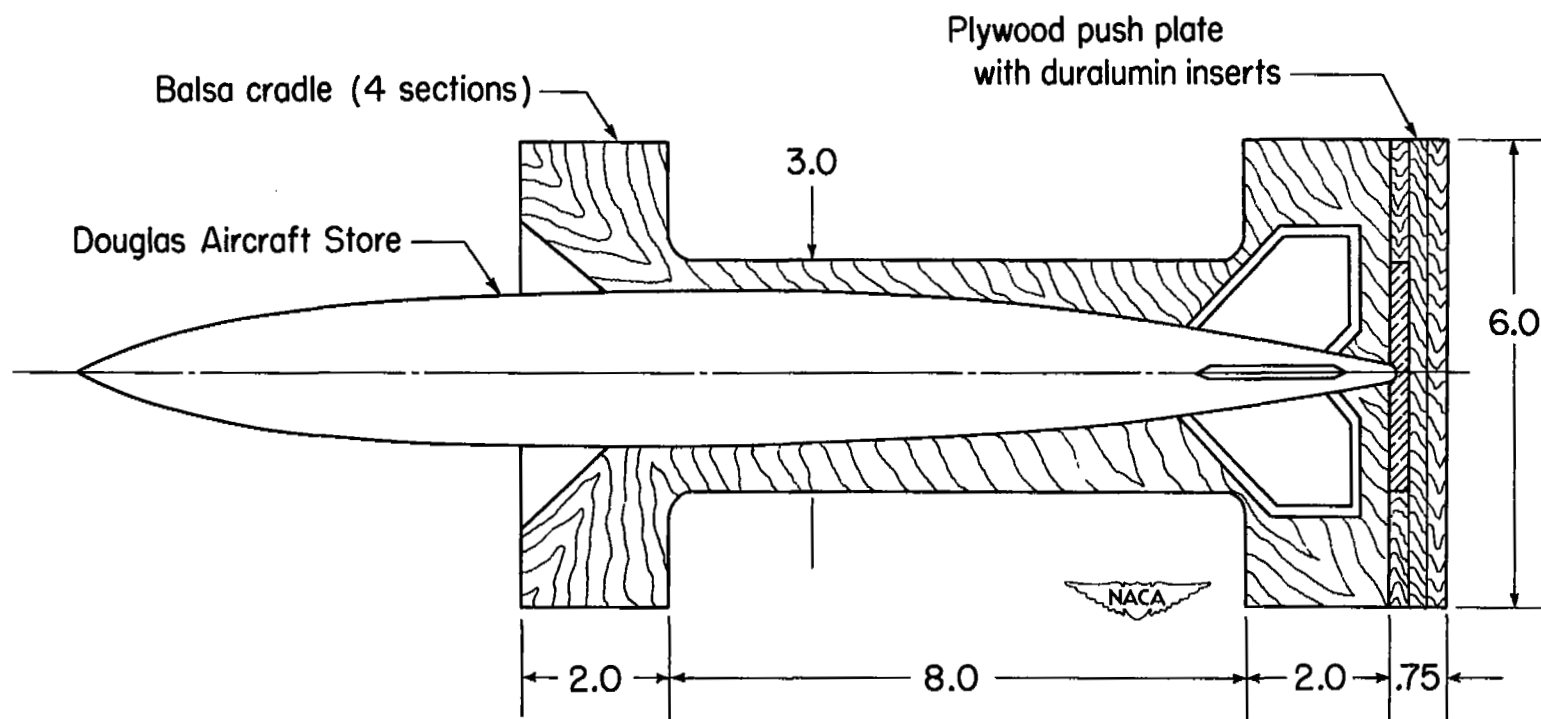
NACA

Figure 8.- Sketch of one of the external stores tested in the compressed-
helium gun.  All dimensions are in inches.

Figure 9.- Compressed-helium gun.

NACA
L-70365.1
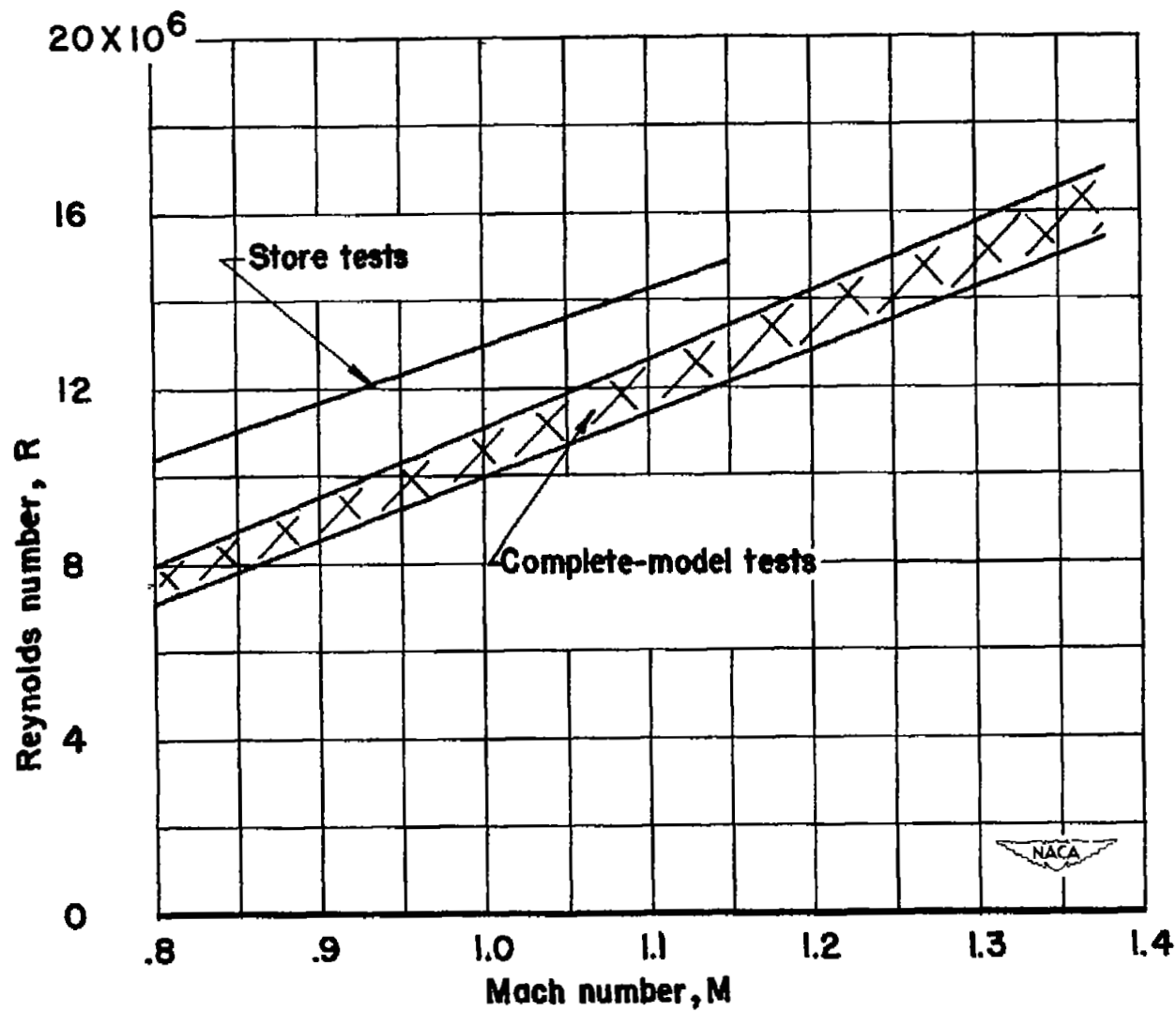
Figure 10.- Variation of Reynolds number with Mach number.
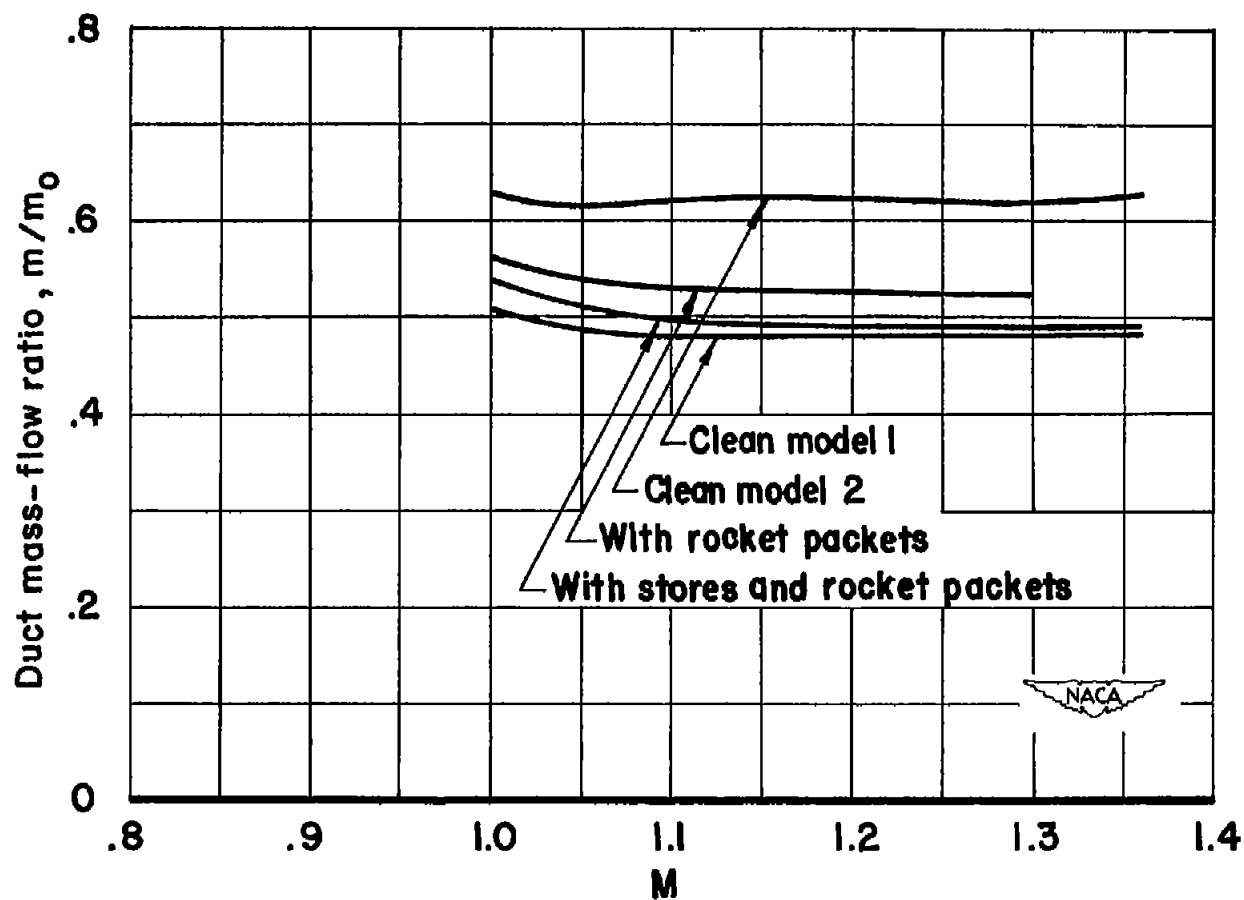
Figure 11.- Mass-flow ratio.
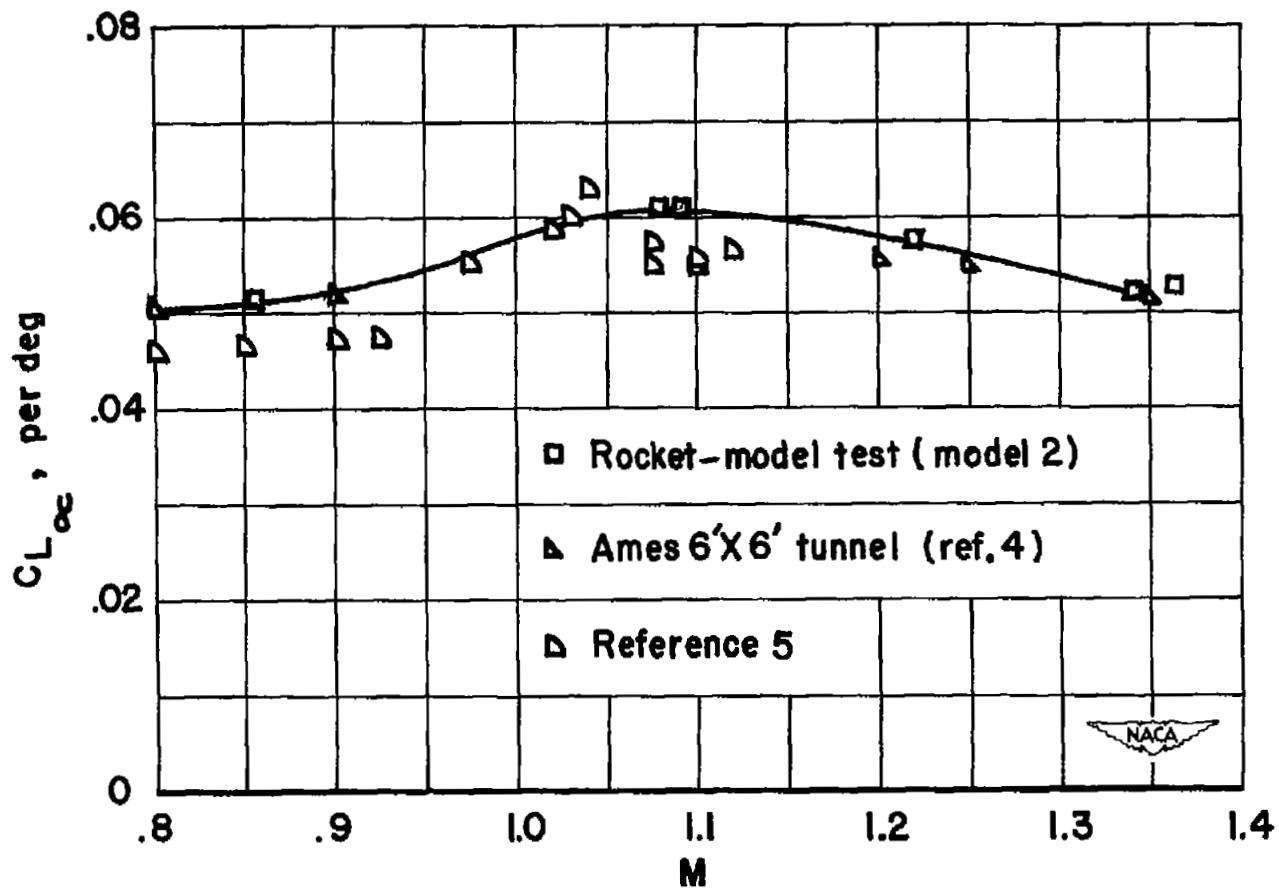
Figure 12.- Lift-curve slope. Fairing based on rocket-model data.
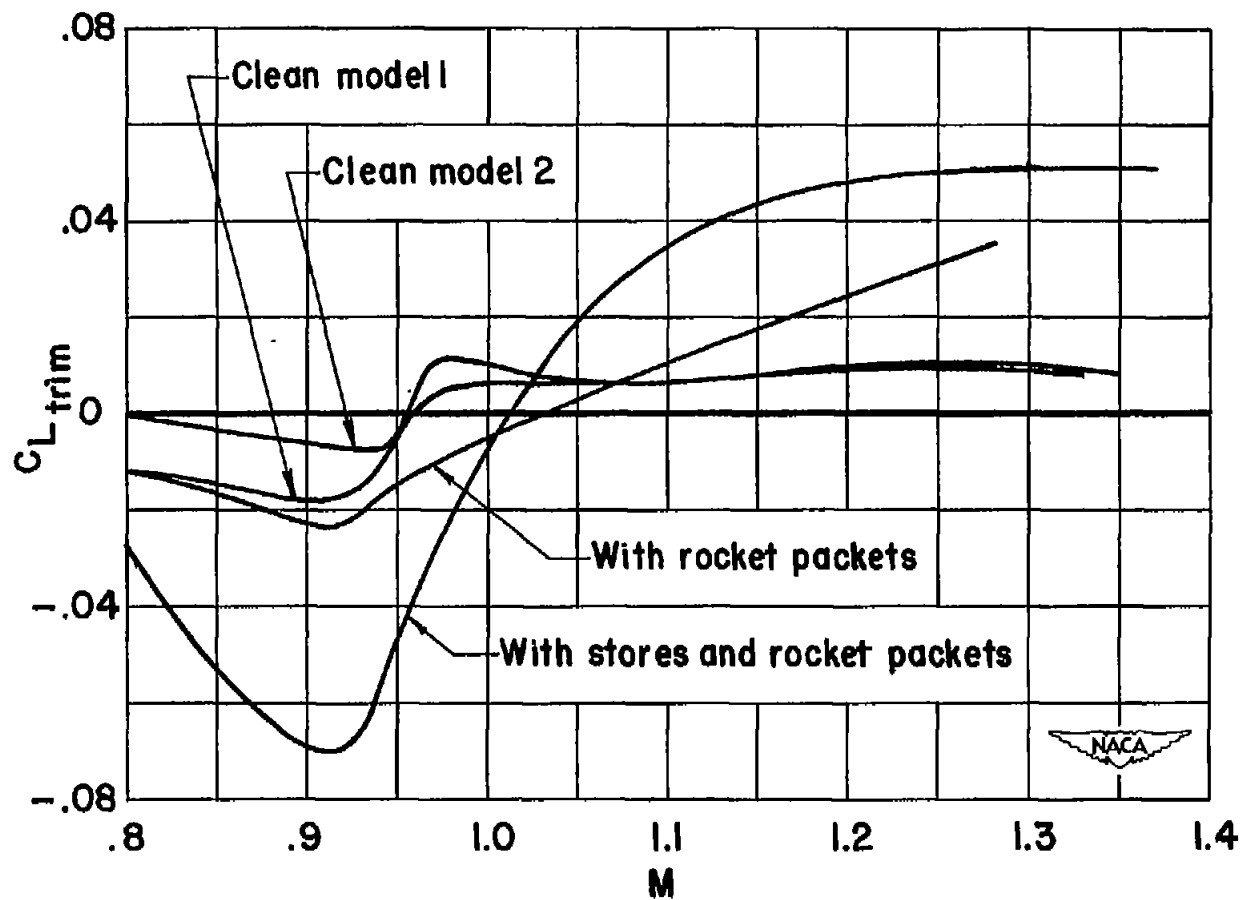
Figure 13.- Trim lift coefficient.
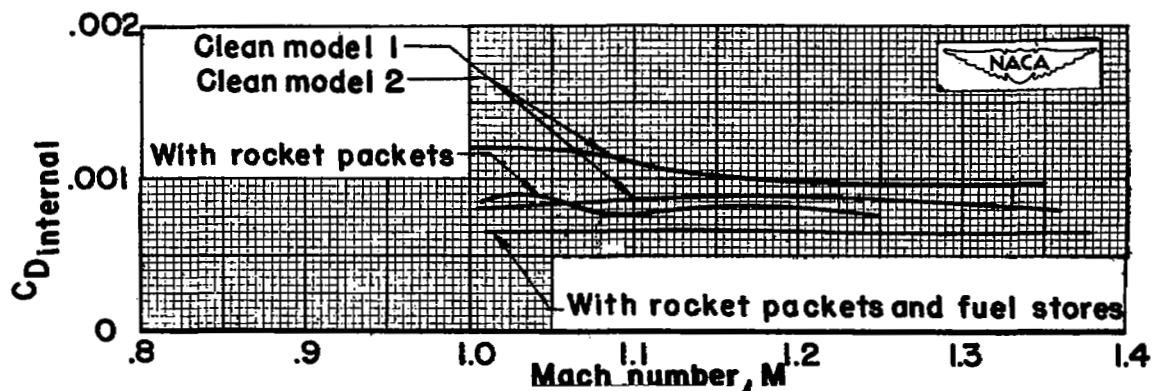
Figure 14.- Internal drag.
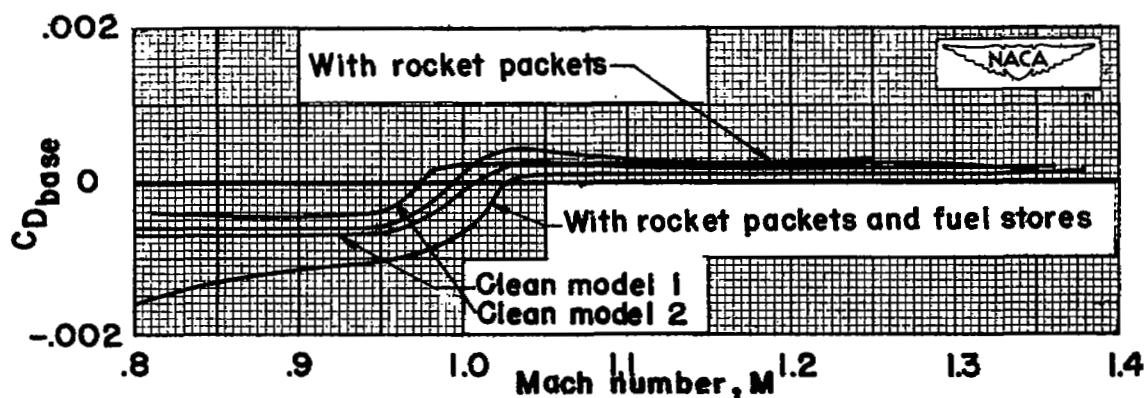


Figure 15.- Base drag (choking cup).
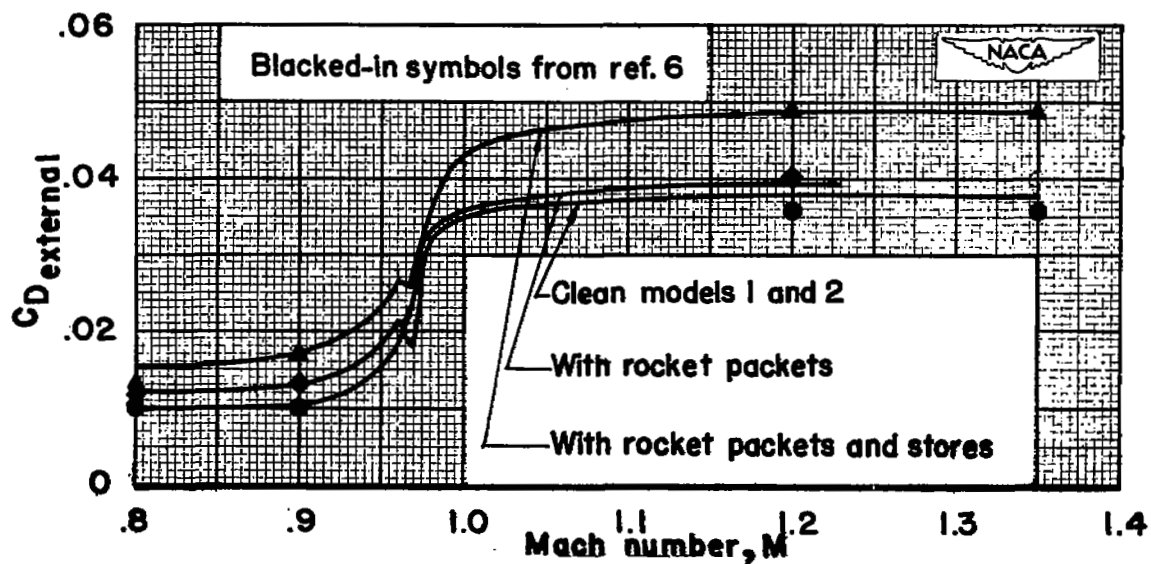


Figure 16.- External drag.
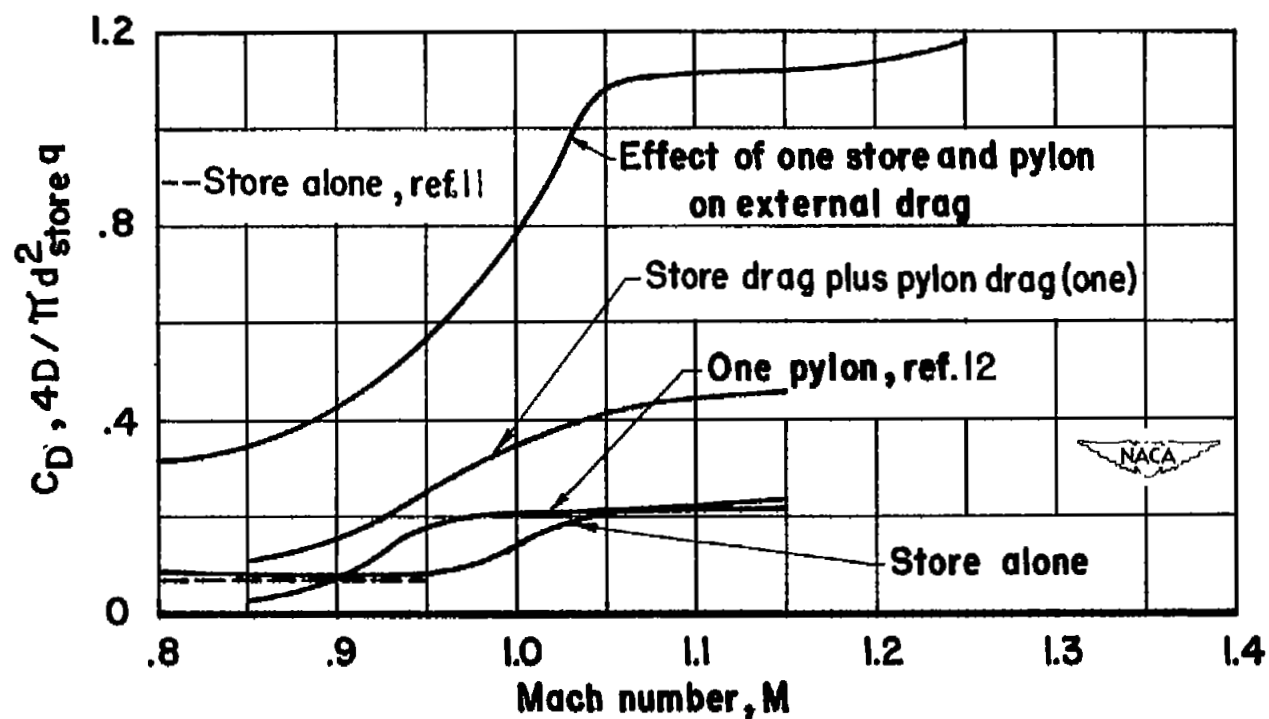
Figure 17.- External-store and store-pylon drag.
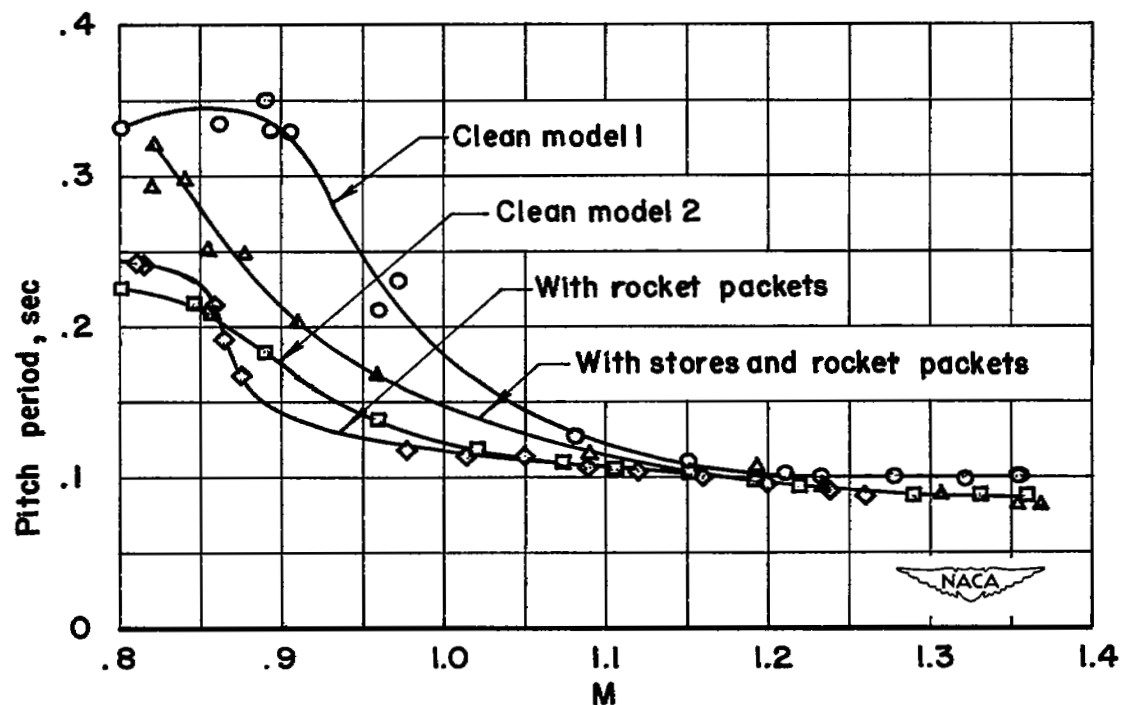
Figure 18.- Pitch period.
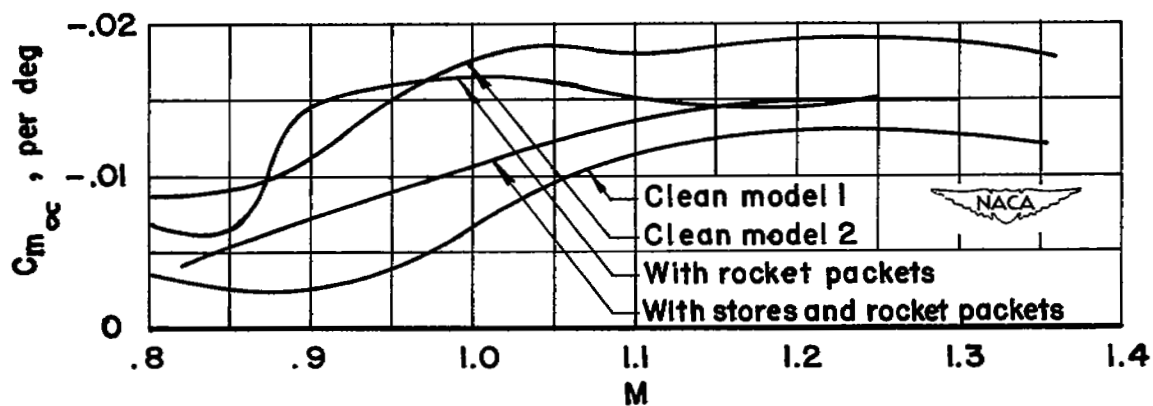
Figure 19.- Longitudinal stability. Center of gravity of clean model 2 located at 0.099c̄; center of gravity of other three models at about 0.17c̄ (see table I).
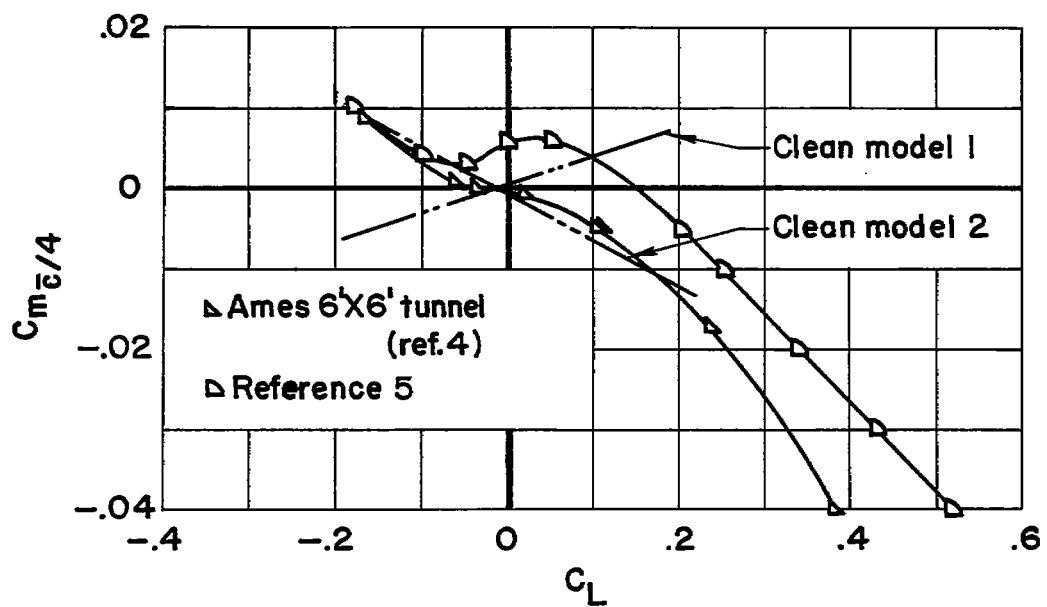
(a) M = 0.9.
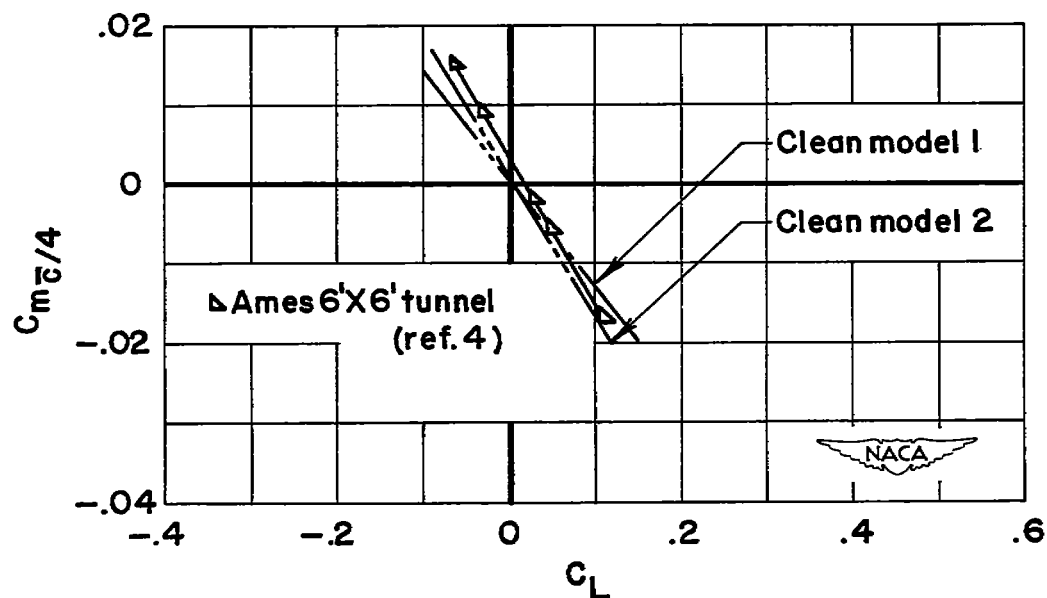
(b) M = 1.2.

Figure 20.- Pitching moment about the quarter chord.
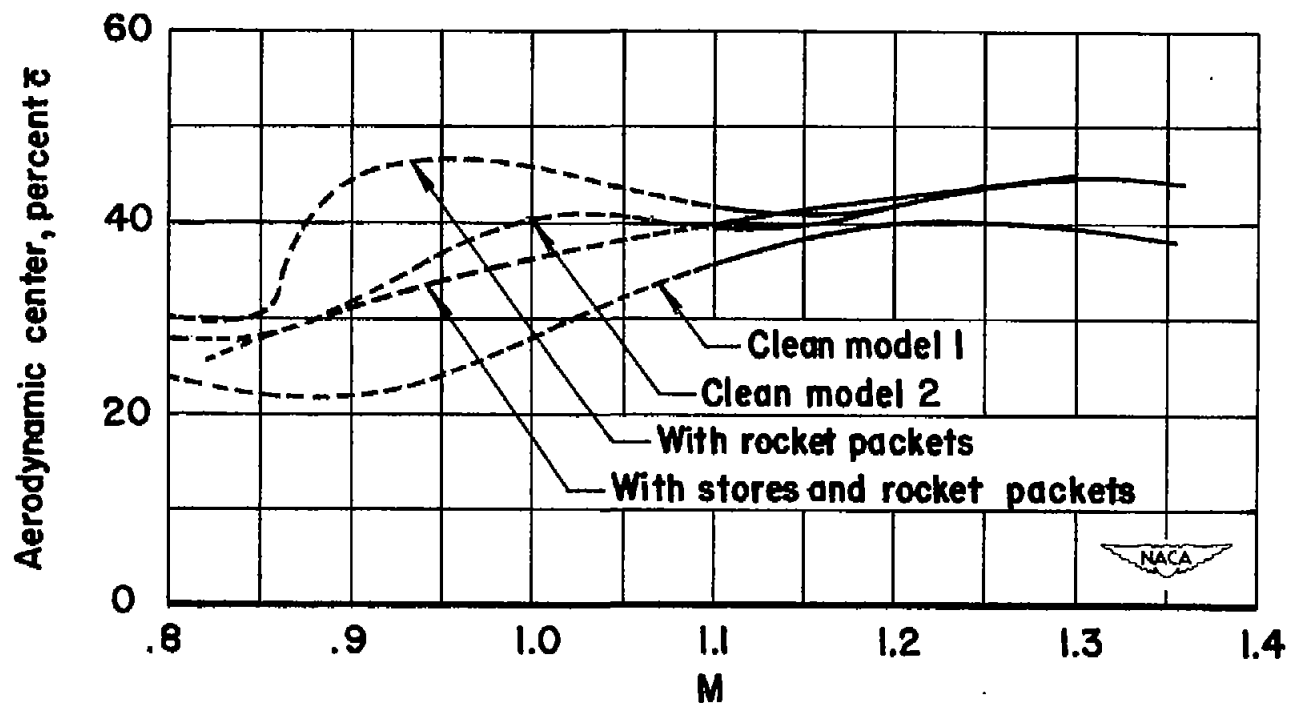
Figure 21.— Aerodynamic-center location.
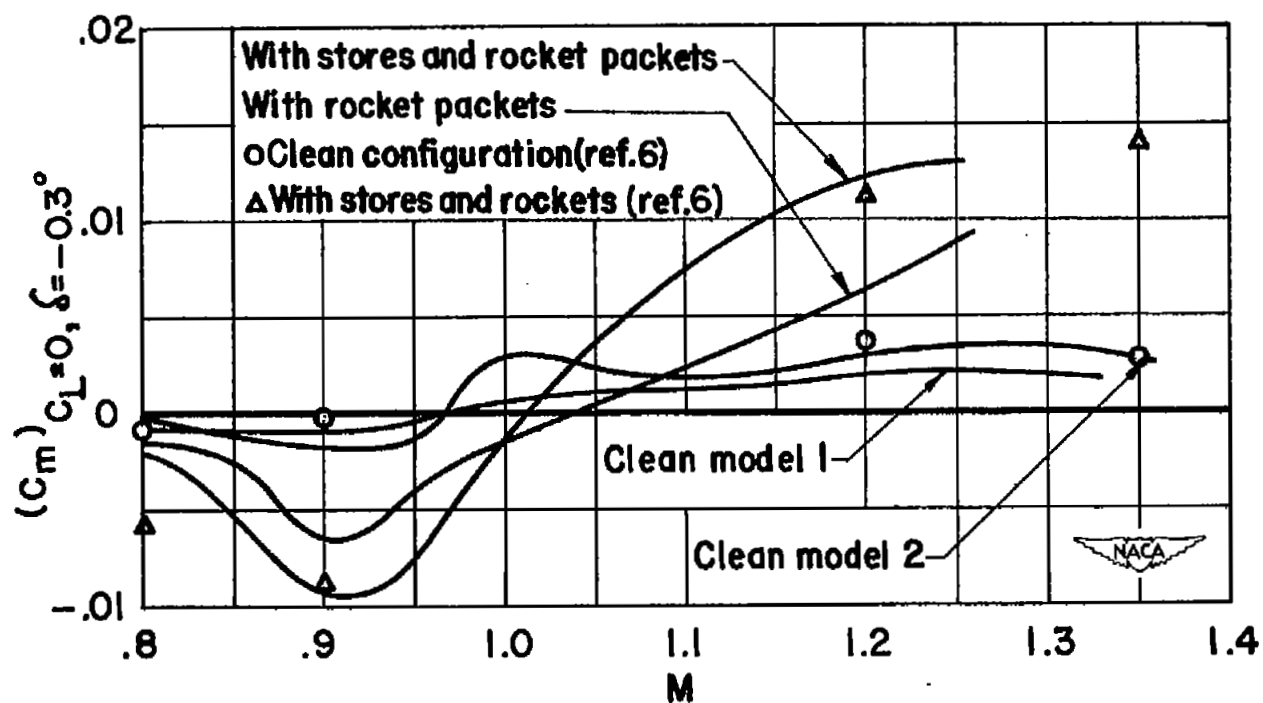
Figure 22.- Pitching moment at zero lift, elevons deflected 0.3°, trailing edge up.

Figure 23.- Time required for the short-period longitudinal oscillation to damp to one-half amplitude.
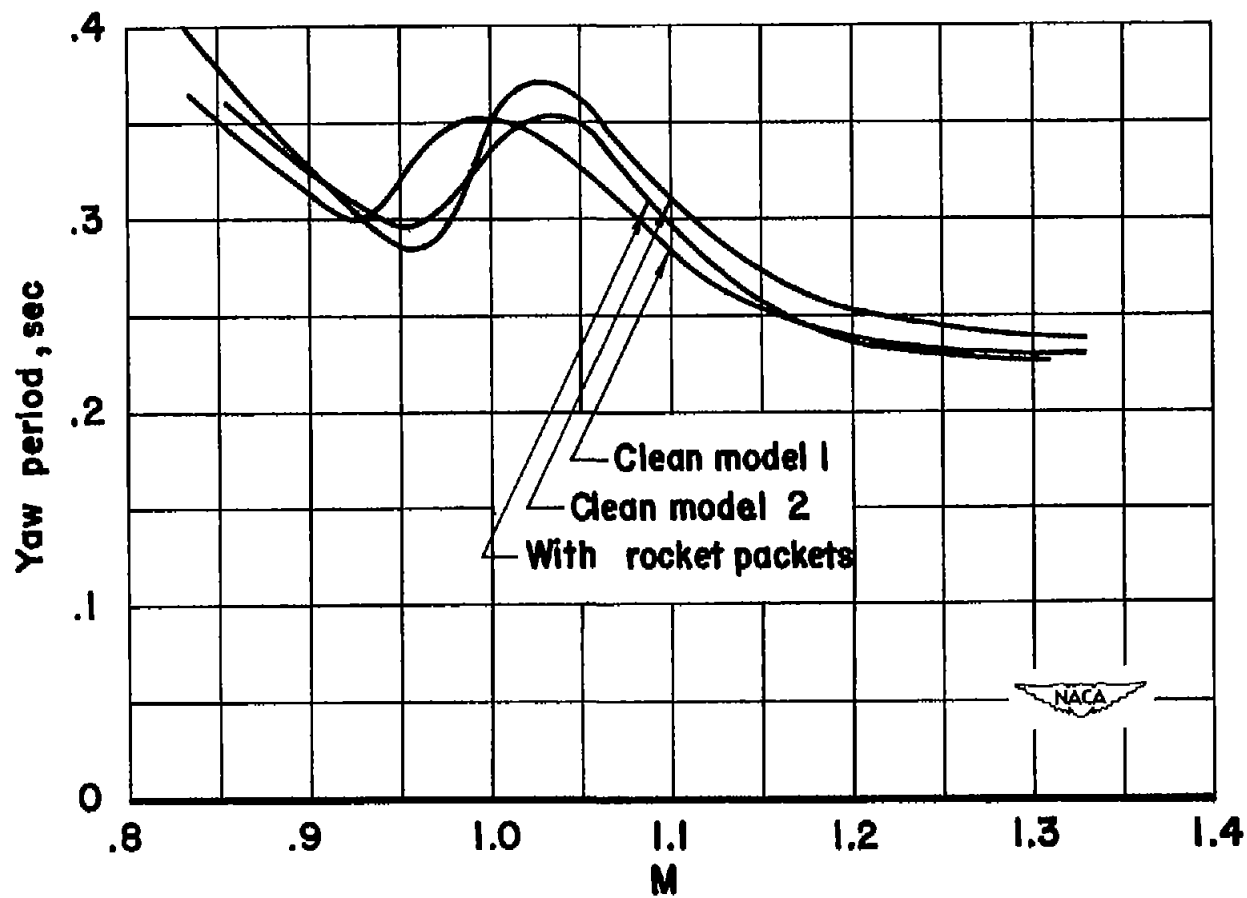


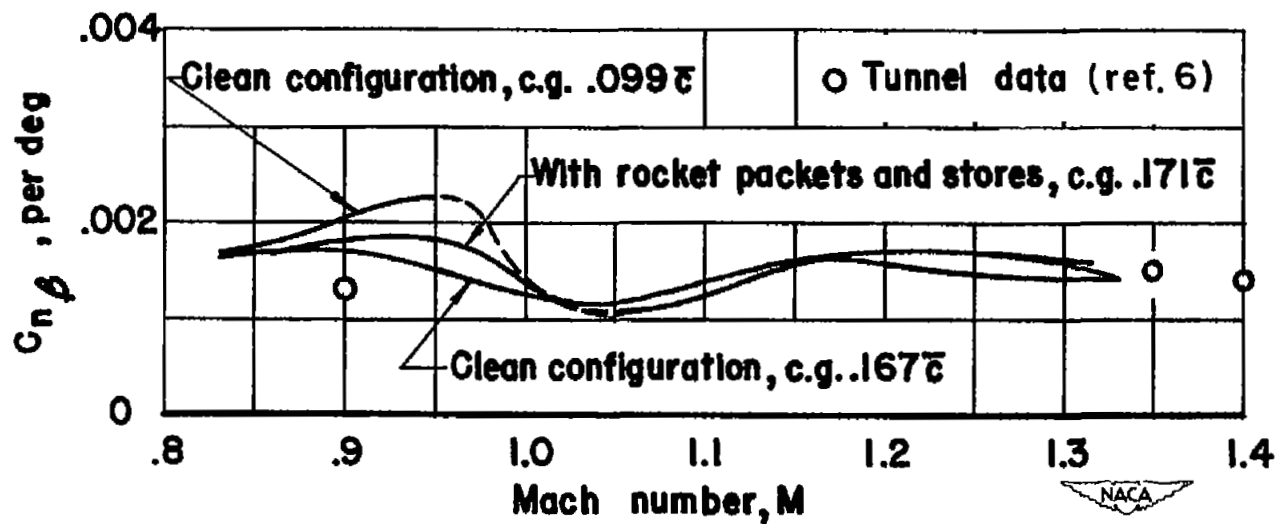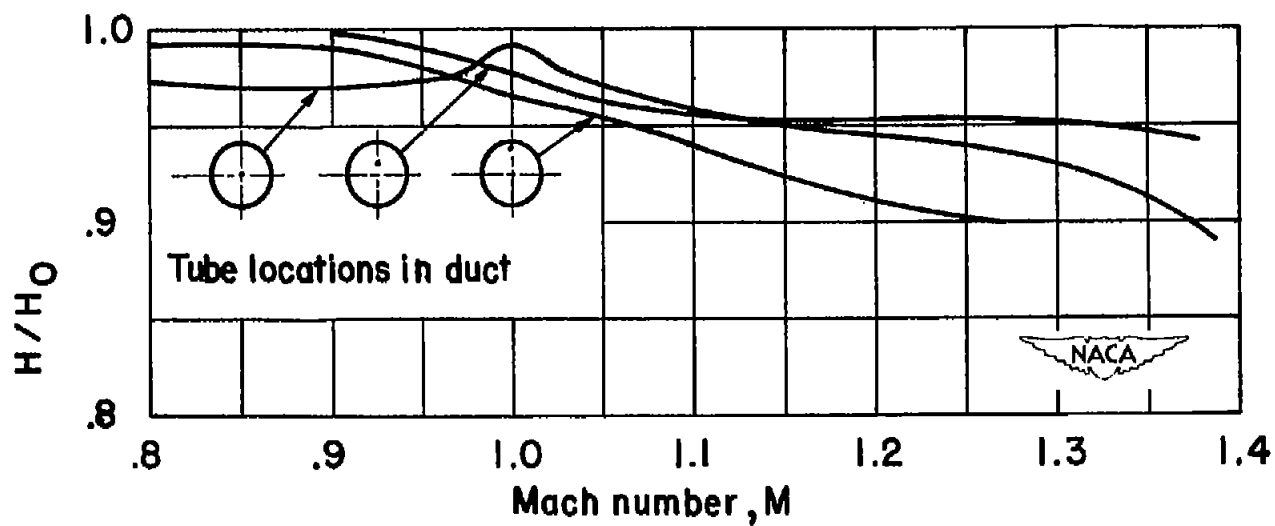Figure 24.- Pitch-damping parameter.

Figure 25.- Yaw period.

Figure 26.- Directional stability.

Figure 27.- Duct total-pressure recovery.